PCCP

PAPER

View Article Online
View Journal | View Issue

Cite this: *Phys. Chem. Chem. Phys.*, 2015, **17**, 17601

Size-dependent electronic structure controls activity for ethanol electro-oxidation at Pt_n/indium tin oxide (n = 1 to 14)†

Alexander von Weber, Eric T. Baxter, Sebastian Proch, Matthew D. Kane, Michael Rosenfelder, Henry S. White and Scott L. Anderson*

Received 28th March 2015,
Accepted 15th May 2015

DOI: 10.1039/c5cp01824b

www.rsc.org/pccp

Understanding the factors that control electrochemical catalysis is essential to improving performance. We report a study of electrocatalytic ethanol oxidation – a process important for direct ethanol fuel cells – over size-selected Pt centers ranging from single atoms to Pt_{14}. Model electrodes were prepared by soft-landing of mass-selected Pt_n^+ on indium tin oxide (ITO) supports in ultrahigh vacuum, and transferred to an *in situ* electrochemical cell without exposure to air. Each electrode had identical Pt coverage, and differed only in the size of Pt clusters deposited. The small Pt_n have activities that vary strongly, and non-monotonically with deposited size. Activity per gram Pt ranges up to ten times higher than that of 5 to 10 nm Pt particles dispersed on ITO. Activity is anti-correlated with the Pt 4d core orbital binding energy, indicating that electron rich clusters are essential for high activity.

Introduction

The electrochemical ethanol oxidation reaction (EOR) has been studied extensively due to interest in developing direct alcohol fuel cells.[1–12] Platinum or platinum alloys are commonly used to catalyze EOR because they are able to break the C–C bond in ethanol to reach the energetically favorable CO_2 product. EOR at Pt in aqueous electrolyte is a complex reaction involving the potential-dependent formation and reaction of multiple reaction intermediates and products. EOR occurs by a heterogeneous inner-sphere mechanism, involving the adsorption of ethanol as the initial step, as documented by previous experimental and theoretical studies.[3–5,12] Absorbed CO and CH_3CO intermediates, and CH_3CHO, CH_3COOH and CO_2 products have been detected during ethanol oxidation by mass spectrometry, chromatography, and vibrational spectroscopies.[3–6,9] The efficiency of EOR is influenced by the electronic and geometric properties of the surface, and can be modulated by alloying with Ru, Sn and other metals.[3,13,14] Additionally, the oxidation of ethanol is sensitive to the surface atomic structure, occurring at different rates on different crystal planes of Pt.[1,2,7]

We report a study focusing on the effects on EOR activity of varying the size of the catalytic Pt centers from 1 to 14 atoms. These small Pt_n clusters have EOR activity per gram Pt that varies strongly and non-monotonically with size. One might expect that varying catalytic site geometries would be important in this size range, however, activity is found to be most strongly dependent on the electronic properties of the clusters, which vary strongly with Pt_n size, as shown by X-ray photoelectron spectroscopy (XPS).

Deposition of size-selected clusters to form model catalytic electrodes allows the size and coverage of the supported catalytic centers to be varied independently, providing mechanistic tools that complement the many detailed studies on single crystal or supported particle electrodes. A number of groups have developed such capabilities, as briefly reviewed in the ESI.† We reported a study of the oxygen reduction reaction (ORR) at Pt_n/glassy carbon,[15] finding that some sizes of Pt_n catalyze oxidation of carbon by water, with such fast kinetics that it is difficult to observe other chemistry. Therefore, the experiments here used indium tin oxide (ITO) electrode substrates.

In that study, we also found that model Pt_n/glassy carbon electrodes exposed to air before the electrochemical studies had activity strongly modified by adventitious adsorbates. It is common in electrochemical studies to remove such adsorbates by repeated potential cycling. For our very small Pt_n clusters, we had concern that potential cycling might cause dissolution or other processes that might broaden the initial size selection. Therefore, the experiments below were done using a vacuum-compatible *in situ* electrochemical cell, with every effort made to minimize exposure to adventitious adsorbates. This experimental arrangement imposes limitations on the complexity of the electrochemical cell, restricting measurements to static conditions.

Department of Chemistry, University of Utah, 315 S. 1400 E., Salt Lake City, UT 84112, USA. E-mail: anderson@chem.utah.edu

† Electronic supplementary information (ESI) available: Description of the materials and methods, of related size-selected electrochemical work and gas-phase cluster experiments, as well as additional data and analysis supporting the conclusions. See DOI: 10.1039/c5cp01824b

As discussed above, the EOR mechanism has been studied using much more elaborate experiments by many other researchers. We, therefore, do not address broader mechanistic issues, but focus our attention on what is unique about our results – the ability to vary the Pt_n cluster size, while keeping all other experimental parameters constant. The issue of possible effects of potential cycling on cluster size is discussed further below.

Experimental methods

The experiments were performed using a cluster beam deposition/surface analysis instrument described previously.[15–17] This instrument consists of a laser vaporization cluster source, a guided ion mass-selecting beamline, and a ultra-high vacuum (UHV) system (base pressure 1×10^{-10} mbar) where samples are prepared and characterized before the electrochemical studies. The main UHV chamber contains the deposition end of the cluster beamline, a spectroscopy station for X-ray and UV photoelectron spectroscopy and low energy ion scattering, and several mass spectrometers for gas-surface reactivity studies. ITO substrates, cleaned as discussed below, are clipped into a substrate holder fabricated from a tantalum backing plate with tantalum spring clips that contact the edges of the front surface of the substrate, and press it against the backing plate. The substrate holder is mounted *via* heating wires to a cryostat, which is mounted on a UHV manipulator, allowing the temperature to be varied between ~100 and 1000 K, as measured by a thermocouple spot-welded to the backing plate. The UHV system includes a valved port that allows a separately pumped antechamber to be attached beneath the main chamber. When the sample is inserted into the antechamber, the cryostat passes through a seal that allows the antechamber to be pressurized or vented. When the lower side of the seal is at atmospheric pressure, the main chamber pressure only rises by $\sim 1 \times 10^{-8}$ mbar.

The *in situ* electrochemical arrangement is similar to one used previously,[15] with the following modifications. A new 2-section antechamber was constructed to allow more space around the electrochemical cell, to facilitate disassembly for cleaning, and to better protect gauges and pumps from electrolyte. A new electrochemical cell was constructed from polyether ether ketone (PEEK), with separate compartments for working, counter, and reference electrodes, separated by glass frits (VitraPOR Borosilicate Glass from ROBU, Inc.). The working compartment is open at one end, to allow it to be mated to the Pt_n/ITO working electrode, sealing *via* an O-ring at the open end of the working compartment. After preparation and characterization of the Pt_n/ITO electrode in the UHV chamber, and insertion into the antechamber, a linear translator was used move the open end of the electrochemical cell into contact, surrounding the cluster-containing spot. To give adequate sealing force, a second linear translator was used to press a Viton-capped rod against the back of the substrate holder. The inside diameter of the working electrode compartment is 3.17 mm, compared to the 2 mm diameter spot containing Pt clusters.

At the bottom of each electrode compartment there are ports fed by PEEK tubes for electrolyte injection, and at the top there are ports for exhaust of gases or excess electrolyte. Between the working and counter electrode compartments, which were filled with the same electrolyte solution, a 5 mm diameter, 2.5 mm thick frit of porosity P3 (16–40 μm pores) was used, sealed in place with an O-ring. To minimize electrolyte mixing between the working and reference electrode compartments, a finer P4 frit (10–16 μm pores) was used. The counter electrode is a cylinder of Pt mesh (>99.9% Pt, Alfa Aesar) lining the inside of the counter electrode compartment, connected to a Pt wire that extends through the electrolyte exhaust port. The reference electrode was a length of AgCl-coated Ag wire. At the start of each experiment, the cell was dry, having been at high vacuum overnight.

One issue for *in situ* electrochemistry is that the reference electrode must be dry when the experiment is started. We used an Ag/AgCl (0.1 M NaCl) electrode, prepared fresh before each experiment as follows. A piece of high-purity Ag wire (>99.9985% Ag, Alfa Aesar) was ultrasonicated for 15 minutes in ethanol and then deionized water, then briefly dipped in 0.1 M HNO_3 to remove oxide,[18] rinsed in deionized water, and then immersed in sodium hypochlorite solution for 20 minutes to establish a chloride layer.[19] The silver wire was then air dried and mounted into the dry electrochemical cell. The Ag/AgCl electrode in 0.1 M NaCl has a formal potential of 0.281 V *vs.* the normal hydrogen electrode (NHE). The potential and stability of the reference electrode was checked against a commercial Ag/AgCl electrode by placing both in a beaker containing 0.1 M NaCl, and it was found that the reference electrode potential was correct and stable within 1.4 ± 0.5 mV over 20 minutes, which is a typical time for the electrochemical part of the experiments. As described below, however, the day-to-day reproducibility of the reference electrode in the *in situ* electrochemical cell was found to be $\sim \pm 14$ mV, and this is taken as the uncertainty in our measured potentials.

The 0.1 M NaCl electrolyte used in the reference compartment was prepared from >99.0% NaCl (Macron Chemicals) and freshly generated 18.2 MΩ cm deionized (DI) water from a Millipore Milli-Q purifier. The electrolyte for the working and counter electrode compartments was 0.1 M $HClO_4$ prepared from 70% $HClO_4$ (Aldrich, 99.999% trace metal basis) dissolved in 18.2 MΩ cm water. All electrolytes were sparged with N_2 in order to remove O_2, the presence of which leads to interfering signal from oxygen reduction. Ethanol was added to the 0.1 M $HClO_4$ solution after sparging. Except as indicated, all experiments were done with 1% ethanol by volume (1% v/v), corresponding to ~0.17 M concentration. Electrolytes were drawn into syringes just before injection into the fill tubes leading to the cell.

After completion of each day's experiment, the cell and antechamber were dismantled, cleaned to remove all traces of electrolytes, and dried. As part of this process, the used Pt_n/ITO electrode was removed and replaced with a fresh ITO substrate, which was cleaned by ultrasonication in ethanol and then 18.2 MΩ cm water[20] followed by air drying. A freshly prepared Ag/AgCl wire was inserted into the reference compartment of the cell. The antechamber was reattached to the main chamber, and then rough-evacuated with a trapped mechanical pump to

remove water or other species adsorbed on surfaces. The antechamber was then evacuated with a turbomolecular pump overnight while the sample was heated to 340 K, to further degas the sample, cell, and antechamber. Because of the large water and ethanol exposures to both the antechamber and cell, the chamber pressure (hot) was typically still $\sim 5 \times 10^{-7}$ mbar by the next morning. At this point the sample was pulled into the UHV chamber, and the antechamber was isolated and allowed to cool, while being pumped by its own turbomolecular pump.

The ITO electrode substrates were prepared by dicing commercial ITO-coated glass plates (Sigma Aldrich, 15–25 Ω square^{-1}, lot MKBN8257V) into 8 × 12 mm rectangles, to fit the substrate holder. To insure good electrical contact with the ITO film, the edges of the substrates were sputter-coated with gold. A Bruker Dimension Icon atomic force microscope (AFM) was used to examine the polycrystalline ITO surface, showing domain sizes on the order of 30 nm, maximum height variation of ~8 nm, and average roughness (R_a) of 1.1 nm, as shown in Fig. 1.

After baking at 340 K overnight, the ITO substrate was pulled into the UHV chamber and characterized by XPS, which showed significant C 1s signal from adventitious adsorbates (Fig. 1). This carbon signal was not removed by heating in UHV to 670 K, or to 600 K in 10^{-5} mbar of O_2 (in the antechamber). The substrate holder can reach much higher temperatures, but we were concerned about thermal decomposition of the ITO, and therefore adopted a different cleaning strategy. Samples were sputtered with 1 keV Ar^+, using the minimum exposure needed to eliminate the C 1s signal, and then annealed at 670 K for 30 minutes in 1×10^{-7} mbar of O_2, in order to produce a fully oxidized surface. As shown in Fig. 1, this process results in carbon-free ITO with In : Sn stoichiometry of ~12 : 1, consistent with the Sn doping level in the ITO. Recently, Klett *et al.*[21] reported use of Ar^+ sputtering to remove carbon from ITO supports for a photoemission study of Pt_n deposited on ITO, the main difference being that they annealed their samples in vacuum, rather than O_2. From our perspective, the most important property of the ITO substrates is that they should be inert, so as to not interfere with measurements of signals from the Pt_n clusters. As shown below, the cleaned ITO substrates showed no activity for EOR or water electrolysis in the potential range of interest.

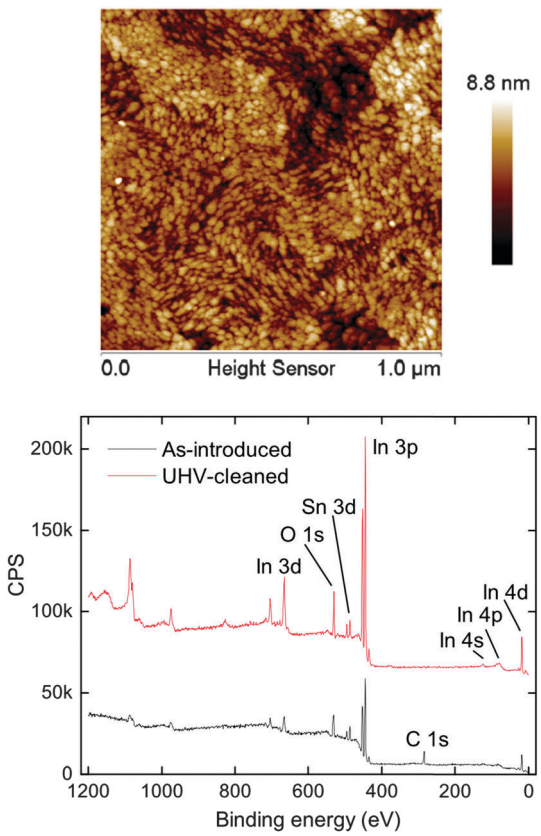

Fig. 1 Top: AFM image of as-received ITO thin film electrode substrate. Bottom: XPS for as-introduced (bottom) and UHV-cleaned (top) ITO.

Pt_n^+ clusters were produced by laser vaporization, formed into a beam, and passed through a quadrupole mass filter to produce a beam containing only a single cluster size, as described elsewhere.[22] The clusters were deposited on the cleaned ITO substrates at a kinetic energy of 1 eV per atom, using a 2 mm diameter mask to define the cluster spot. The cluster coverage was monitored continuously during deposition by measuring the neutralization current of the Pt_n^+, and deposition was stopped when the desired coverage was reached. To allow data for different cluster sizes to be compared directly, each sample contained 4.40×10^{12} Pt atoms deposited in the 2 mm diameter spot, the only difference being the size of clusters deposited. This coverage (1.5×10^{14} cm^{-2}) is equivalent to ~0.1 of a close-packed Pt monolayer, and typical deposition times were 5–10 minutes.

One obvious question is the extent to which the deposited cluster size is retained after deposition and under electrochemical cycling. The roughness of the ITO support precludes detection of subnanometer clusters by AFM or STM. As shown below, the XPS binding energies oscillate strongly with deposited cluster size, indicating that the Pt_n/ITO retain memory of the deposited size.

We also used scanning transmission electron microscopy/high angle annular dark field imaging (STEM/HAADF) to examine size-selected Pt_n deposited on lacey carbon TEM grids. Grids were prepared by depositing ~4% of a ML of Pt in the form of Pt_1, Pt_7, or Pt_{14}, which were then transferred in air, and imaged using a JEOL JEM 2800 microscope. Selected area energy dispersive X-ray spectroscopy (EDS) was used to verify that the observed spots were, indeed, due to Pt. The images are shown in Fig. 2. There are several points to note and which are discussed further in the ESI.† The size and contrast of the spots and their spacings on the grids, are consistent with the deposited Pt_7 and Pt_{14} remaining intact, rather than breaking up or sintering on the carbon TEM grids. The image for the grid prepared by Pt_1 deposition, in contrast, shows no obvious structure. It is not surprising that we were unable to image single Pt atoms using this non-aberration-corrected instrument, however, this negative result provides the important insight that deposited atoms do not diffuse and sinter to form clusters large enough to be observed in the images. The conclusion is that at least for Pt_n on carbon under the conditions

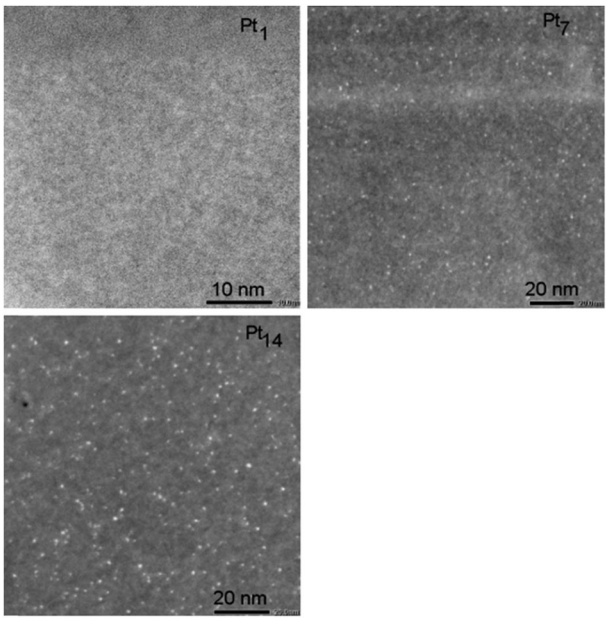

Fig. 2 S/TEM images of lacey carbon TEM grids prepared by deposition of ~4% of a monolayer of Pt as: top left: Pt_1, top right: Pt_7, and bottom: Pt_{14}. Note differences in scale.

studied, there is no evidence of efficient agglomeration of either clusters or deposited atoms.

The important question, however, is whether the clusters remain intact on ITO under electrochemical potential cycling. Fortunately, the results, themselves, provide strong evidence regarding this issue. The electrochemical activities are found to oscillate with cluster size, and the oscillations are strong and sharp enough to imply that the deposited clusters must remain within a few atoms of the deposited size. Furthermore, there is no evidence that the size distribution broadens significantly during the sequence of CVs used to probe the activity of the Pt_n/ITO. This issue is discussed further below.

Immediately after cluster deposition, the samples were characterized by XPS. Because the 0.1 ML Pt coverage results in weak signal, and the Pt 4f peaks have strong and energy-dependent background from the ITO support, Pt was detected *via* its 4d peaks, with a typical spectrum (Pt_{10}/ITO) shown in Fig. S1 (ESI†). The $4d_{5/2}$ peak partially overlaps the 2s peak from argon implanted during ITO cleaning, and to avoid any possible influence on the fitting process, the BEs given below are for the Pt $4d_{3/2}$ peak.

After XPS, the samples were inserted into the antechamber, which was then vented with UHP argon to a pressure above atmospheric pressure, to avoid air intrusion through the electrolyte injection tubes. The electrolyte tubes were then uncapped and connected to syringes for injection. The 0.1 M $HClO_4$ electrolyte containing 1% ethanol was first injected into the working electrode compartment with the cell pulled back from contact with the Pt_n/ITO electrode. Electrolyte was injected until a meniscus protruded from the open end of the cell, which was then moved into contact with the sample. Additional electrolyte was injected until it was observed to flow from the exhaust port at the top of the compartment. The same electrolyte solution was then injected into the counter electrode compartment, and finally 0.1 M NaCl electrolyte was injected into the reference electrode compartment.

Once the cell was filled, the EOR was studied by running a series of cyclic voltammograms (CVs) over increasing potential ranges: −0.3 V to 0.5 V, −0.3 V to 0.7 V, −0.3 V to 0.8 V, −0.3 V to 1.0 V, and finally −0.3 V to 1.3 V, all measured with respect to the Ag/AgCl reference electrode. The scan ranges were chosen based on several considerations. The lower potential limit was chosen to allow us to observe the onset of the hydrogen evolution reaction (HER) for purposes of calibrating the reference electrode potential (see below), but without generating enough H_2 to cause bubble formation, which is a problem for our small diameter cell. Another consideration is the possibility that very small Pt clusters might dissolve, particularly when the CVs are scanned over potential ranges where Pt oxidation and reduction occur. This motivated the initial scans, which remained below the potential where Pt_n oxidation might be expected. The final upper potential limit was chosen to avoid formation of O_2 bubbles from the oxygen evolution reaction (OER).

All reported potentials have been converted to V *vs.* NHE (potential relative to the normal hydrogen electrode) using the following procedure. Nominally, potentials measured against our reference electrode (Ag/AgCl 0.1 M NaCl) should be converted to potentials *vs.* NHE by adding 0.281 V, however, the use of an initially dry reference electrode raised concern about the day-to-day reproducibility of the reference potential. Therefore, to provide an internal reference, the lower potential limit for all CVs was chosen to allow observation of both the onset of the H_2 evolution reaction (HER) and the peak due to H_2 oxidation. To bring these features to their literature values[23] required, on average, a shift of 0.284 V – quite close to the 0.281 V nominal shift. More importantly, the day-to-day variation in the shift was up to ±14 mV, which we take as an estimate of the uncertainty in the measured potentials. The potential axis of the CVs have all been adjusted to bring the potential of the HER onset and H_2 oxidation peak to the literature value. Note: because the Ag/AgCl electrode was used to control the CVs, the scan range relative to NHE varied by up to ±14 mV from sample to sample.

An example of the initial variable width CVs (0.1 V s^{-1} scan rate) is shown for Pt_{10}/ITO in Fig. S2 (ESI†). In terms of potential *vs.* NHE, the lower potential limit was −0.016 V, and the upper potential limits varied up to 1.58 V. Because the CVs were actually measured against the Ag/AgCl reference electrode, which had ±14 mV day-to-day variations, the exact potential range *vs.* NHE varied slightly from sample to sample. No significant EOR currents were observed until the upper potential was 1.25 V, and the EOR peaks became large only for the CV run over the "full range" of potentials (−0.016 V to 1.58 V). This behavior is in contrast to bulk Pt electrodes, where EOR activity can been seen in CVs where the upper potential does not exceed 1.2 V.[3,5–7] Next, each Pt_n/ITO sample was probed by a sequence of full range CVs, continuing until the EOR signals disappeared.

It is important to note that while the Pt_n/ITO cluster experiments were performed with every effort made to avoid exposure to adventitious adsorbates, it is impossible to completely avoid

this problem. During cluster deposition and XPS characterization in the UHV chamber, the main background species present were CO and water. CO is always present in the UHV background and sticks well to small Pt clusters on oxide supports,[22] desorbing between 400 and 600 K. The water background is elevated ($\sim 1 \times 10^{-9}$ mbar) after the O_2-annealing process used in ITO cleaning, and in addition, the antechamber pressure at the time of sample introduction was in the low 10^{-7} mbar range, also mostly due to residual water from washing the cell and antechamber after each day's experiments. Given that we immediately flooded the cell with electrolyte after introduction to the antechamber, the water exposure is not considered to be a problem, however, binding of CO or other strongly-binding contaminants could partially passivate the Pt surfaces.

To test for the presence of UHV-adsorbed contaminants, a sample was prepared using the same procedure as in the electrochemical experiments, and then examined by temperature-programmed desorption (TPD), where the sample was heated at 3 K s^{-1} while monitoring desorption of water, CO, CO_2 using a differentially-pumped mass spectrometer. The temperature was monitored by a thermocouple spot-welded to a tantalum backing plate behind the ITO substrate, however, it is unlikely that the substrate temperature lagged the measured temperature by more than $\sim$10–20 K, because the substrate was spring loaded tightly against the backing plate. The result of this TPD experiment was that essentially no desorption signal was observed below 650 K, *i.e.*, in the range where CO is known to desorb from Pt_n/alumina,[22] suggesting that the adventitious adsorbate exposure level was low during cluster deposition.

For comparison to the Pt_n/ITO results, analogous experiments were done for polycrystalline Pt ("Pt_{poly}"), for an ITO electrode prepared with $\sim$5–10 nm diameter Pt particles ("Pt_{nano}/ITO"), and for Pt-free ITO. The preparation of these "control" electrodes is described in the ESI.†

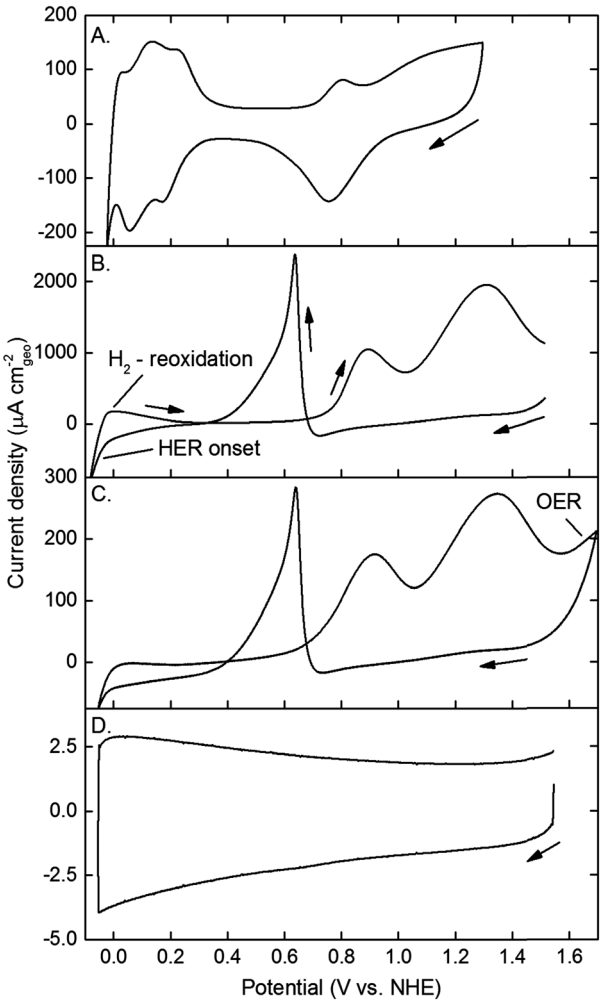

Fig. 3 (A) CV of Pt_{poly} in O_2- and ethanol-free 0.1 M $HClO_4$. (B) CV of Pt_{poly} in O_2-free 0.1 M $HClO_4$ containing 1% by volume of ethanol. (C) CV of Pt_{nano}/ITO in O_2-free 0.1 M $HClO_4$ containing 2% by volume of ethanol. (D) CV of Pt-free ITO in 0.1 M $HClO_4$ containing 1% by volume of ethanol. All acquired at 0.1 V s^{-1} scan rate.

Results

"Control" electrodes

Fig. 3 shows CVs from several control experiments relevant to interpretation of the EOR results.

Fig. 3A shows the CV for Pt_{poly} in N_2-saturated 0.1 M $HClO_4$, without ethanol, which is in good agreement with literature results.[24] At the 1.3 V starting potential, the Pt surface is oxidized, and the peak observed at 0.75 V during the negative-going scan is due to reduction of the oxidized surface. Below 0.3 eV, small peaks are observed for $H^+_{aq} \rightarrow H_{ads}$, and then a sharp onset is observed near 0.0 V for the HER reaction. As the potential is scanned back toward 1.3 V, the structure below 0.3 V corresponds to re-oxidation of H_2 and then $H_{ads} \rightarrow H^+_{aq}$. The structure above 0.8 V is due to oxidation of the Pt surface.[25]

Fig. 3B shows a CV for Pt_{poly} under EOR conditions, which is also similar to results in the literature.[7–9] During the positive-going scan, an oxidation peak is observed at 0.89 V with a background-subtracted current density of 0.9 $\pm$ 0.2 mA cm^{-2}, and then a second oxidation peak is observed at 1.3 V with a current density of 1.8 $\pm$ 0.3 mA cm^{-2}. These features will be referred to as the 1st and 2nd oxidation peaks. The peak currents were estimated by subtracting non-EOR background currents estimated from the CV for Pt_{poly} without ethanol (Fig. 3A), and the uncertainty is due to the uncertainty in the wetted area on the electrode. The current densities for both the 1st and 2nd oxidation peaks have been reported to increase with ethanol concentration, and are thus associated with the oxidation of ethanol.[3–7] Based on vibrational spectroscopy, mass spectrometry and chromatography, the 1st oxidation peak is reported to yield acetaldehyde and acetic acid and a small amount of CO_2, while the 2nd oxidation peak is associated predominantly with the electrogeneration of acetic acid. EOR declines at potentials above $\sim$1.3 V because of Pt oxidation and poisoning by product species.[1,2,5,6] As the potential is scanned back toward negative potentials, a small negative-going feature is observed starting at $\sim$0.9 V *vs.* NHE that is associated with the reduction of the oxidized Pt surface ("PtO_x"). In absence of

ethanol (Fig. 3A) the current from reduction of PtO_x peaks around 0.75 V (-142 μA cm^{-2}), and continues to ~0.5 V. When ethanol is present (Fig. 3B), there is still a PtO_x reduction peak at ~0.73 V (-165 μA cm^{-2}), however, reduction reactivates the Pt surface for EOR catalysis, and the signal below ~0.68 V is dominated by a sharp "reactivation" peak at 0.64 V *vs.* NHE with amplitude of 2.45 ± 0.5 mA cm^{-2}. The reactivation peak is quite sharp, and shows evidence of a shoulder to lower potentials. Near 0.0 V, signals are also seen for HER and H_2 oxidation, but there are no longer distinct peaks between 0.3 and 0.0 V for $H^+ \leftrightarrow H_{ads}$, presumably because adsorption of ethanol and its reaction intermediates blocks many of the Pt sites.[7,8]

Fig. 3C shows a CV for Pt_{nano}/ITO with 2 vol% ethanol in the 0.1 M $HClO_4$ electrolyte. The same three peaks characteristic of EOR are observed: the 1st oxidation peak at 0.92 V *vs.* NHE with current density of 175 ± 30 μA cm^{-2}, the 2nd oxidation peak at 1.34 V *vs.* NHE with current density of 273 ± 43 μA cm^{-2}, and the reactivation peak at 0.64 V *vs.* NHE with peak current density of 284 ± 60 μA cm^{-2}. The example CV for Pt_{nano}/ITO was scanned to somewhat higher potential than that for Pt_{poly}, allowing the onset of the OER to be seen. The maximum current densities for the three EOR peaks for Pt_{nano}/ITO are roughly 7 times lower than those for the analogous Pt_{poly} EOR peaks, but lower current densities are expected for Pt_{nano}/ITO, because only a fraction of the surface is covered by Pt. Fig. 3D shows a CV recorded under identical conditions for a "blank" ITO electrode that was cleaned by Ar sputtering and annealing in O_2 in the UHV chamber, but without Pt_n deposition.

Over the potential range of interest for EOR, the CV is featureless, with 3 to 5 μA cm^{-2} of capacitive current attributed to charging of the double layer. There are no EOR peaks, nor are sharp onsets for HER or OER observed. The implication is that any peaks seen for the Pt_n/ITO electrodes in this potential range can be attributed to reactions catalyzed by the Pt_n clusters.

Coverage dependence for Pt_1/ITO

Fig. 4 shows CVs for model electrodes prepared by deposition of Pt_1 on ITO at 0.05 ML and 0.1 ML coverage. Coverage effects were studied for Pt_1 because two factors suggest that deposited atoms may be more prone to agglomeration than pre-formed, deposited clusters. The average spacing between Pt_n impact positions varies as $n^{-1/2}$ (~0.9 nm for Pt_1 at 0.1 ML), thus the diffusion distances required for agglomeration increase with cluster size. In addition, from consideration of the number of bonds that must be broken, we might expect that the activation energy for diffusion of single atoms on a support should be smaller than those for diffusion or breakup of existing clusters. Indeed, STM,[26,27] ion scattering,[28–31] and reactivity studies[22] all indicate that noble metal atoms on oxides are substantially more prone to diffusion and agglomeration, compared to pre-formed, deposited clusters, even as small as dimers.

As shown in the next section, the activity of electrodes prepared by Pt_n deposition increases dramatically as n varies from 1 to 4 atoms. Therefore, if deposited Pt_1 agglomerate significantly, we would expect to see EOR currents that vary non-linearly with Pt_1 coverage, because higher coverage should result in more cluster formation. Conversely, if deposited Pt_1 do not agglomerate, the EOR currents should simply be linear in coverage.

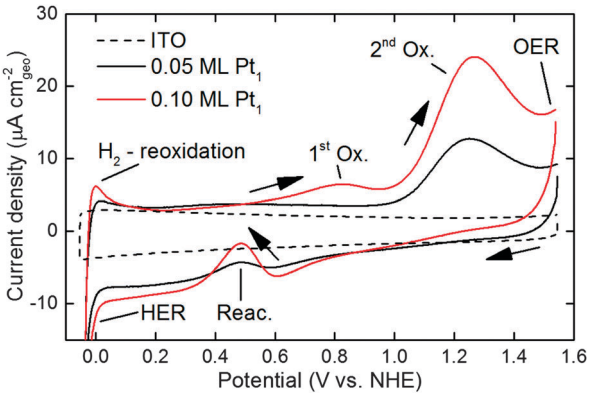

Fig. 4 CVs for Pt_1/ITO at 0.05 ML and 0.01 ML coverages, and for ITO, acquired at 0.1 V s^{-1} scan rate.

The results in Fig. 4 are plotted as current densities to allow comparison with the current densities for the control electrodes (Fig. 3). The measured currents were simply divided by the area of the 2 mm diameter cluster-containing spot (0.031 cm^2), thus this area is mostly ITO with 0.05 or 0.1 ML Pt coverage. For comparison, the current density for a Pt-free ITO substrate is also shown in Fig. 4. The ITO contributes 3 to 5 μA cm^{-2} of structureless current, thus the peaks and other features can all be attributed to Pt deposition.

First consider the higher, 0.1 ML coverage results. Taking the contribution from ITO into account, this CV shows all the same features as the CVs for Pt_{poly} and Pt_{nano}/ITO (Fig. 3B and C, and literature[3–7]), albeit with reduced intensities, as expected from the much lower Pt coverage. Features include the 1st and 2nd oxidation peaks at ~0.82 V and ~1.28 V on the positive-going sweep, and an increase in current above ~1.5 V attributed to the oxygen evolution reaction (OER). On the negative-going scan, reduction of the oxidized Pt starts at ~0.8 V, enhancing activity for EOR catalysis, and resulting in the reactivation peak at ~0.48 V. At lower potentials, current is observed near 0 V for the hydrogen evolution reaction (HER) and H_2 oxidation. For the 0.05 ML coverage electrode, the CV structure is similar, with the exception that there is no distinct peak at the potential expected for the 1st oxidation peak.

For quantitative comparison, it is necessary to subtract the non-EOR background currents that result from the ITO support and from Pt oxidation/reduction (Fig. S3, ESI†). The background-corrected peak current densities at 0.1 ML coverage are ~2.3, 17.2, and 5.3 μA cm^{-2}, respectively, for the 1st and 2nd oxidation and reactivation peaks. For 0.05 ML coverage, the corresponding currents are ~0, ~5.9, and ~1.5 μA cm^{-2}, respectively.

The absence of a distinct 1st oxidation peak at 0.05 ML coverage suggests either that the responsible reactions do not occur on isolated Pt atoms, or that the chemistry occurs over a broader potential range, such that a peak is no longer evident. In that case, the presence of a distinct 1st oxidation peak at 0.1 ML coverage suggests that there was enough agglomeration

at the higher coverage to produce clusters capable of catalyzing this chemistry in the expected potential range. Note however, that even for the higher coverage, this peak is substantially smaller than those observed for Pt_n/ITO prepared with small clusters, suggesting that a substantial fraction of the deposited Pt_1 remain isolated, even at the higher coverage.

Size effects for Pt_n/ITO

Fig. 5 compares CVs recorded under identical conditions, for samples prepared by deposition of Pt_n, n = 1, 2, 4–10, at 0.1 ML coverage. All three EOR peaks increased substantially as deposited cluster size was increased between Pt_1 and Pt_4, decreased to a minimum for Pt_7–Pt_8, then increased again for Pt_9 and Pt_{10}. Despite the large variations in EOR currents, there was little effect of cluster size on the peak potentials. The 1st oxidation and reactivation peak potentials were nearly size-independent, while the 2nd oxidation peak was at ~1.28 V for Pt_1, Pt_7, and Pt_8 (the least active sizes) compared to 1.24 to 1.25 V for the more active sizes.

Fig. 6 summarizes the background-subtracted EOR peak currents, normalized to the mass of Pt present. For Pt_1 the CV for 0.05 ML coverage (7.3×10^{-10} g Pt) was used; all others had 0.1 ML coverage (1.46×10^{-9} g Pt). The error bars are standard deviations of repeated measurements. All three peaks show similar oscillations with cluster size, consistent with the raw CVs in Fig. 5. Pt_1, Pt_7, and Pt_8 have the lowest activities, and Pt_4 and Pt_{10} have activities two to ten times higher. The figure also plots the Pt $4d_{3/2}$ binding energies (BEs) measured for each sample after deposition. The BEs show large (1.5 eV) oscillations with cluster size, which are anti-correlated with the EOR activities (note inverted BE scale).

Fig. 7 shows how the EOR peak currents varied during the sequence of CVs obtained for two samples, and Fig. S4 (ESI†) gives two more examples. The insets to each figure show raw CVs at selected points during the sequence. The intensities of the 1st and 2nd oxidation peaks were at or near their maximum values at the beginning of each CV sequence, while the reactivation peak intensities were initially near zero. Over the course of the first 10–12 CVs, the reactivation peaks increased rapidly, while the intensity of the 2nd oxidation peak decreased, and the 1st oxidation peak was roughly constant. Apart from changes in peak intensities, the qualitative CV structure was similar during these initial CVs.

The oscillatory pattern shown in Fig. 6 was taken from CVs measured just after this initial period of rapid change. To demonstrate that the strong Pt_n size dependence and anti-correlation of EOR activity with Pt 4d BE is not an artifact of the CVs chosen for analysis, Fig. S5 (ESI†) shows similar analysis based on the 2nd CV measured for each sample. The same pattern of activity variations with cluster size is seen, as is the anti-correlation of activity with the Pt 4d BE. The reactivation peak intensities are not shown, simply because they were too small for accurate background subtraction.

The behavior after the initial dozen CVs varied somewhat from sample to sample. In all cases the rate of change in EOR

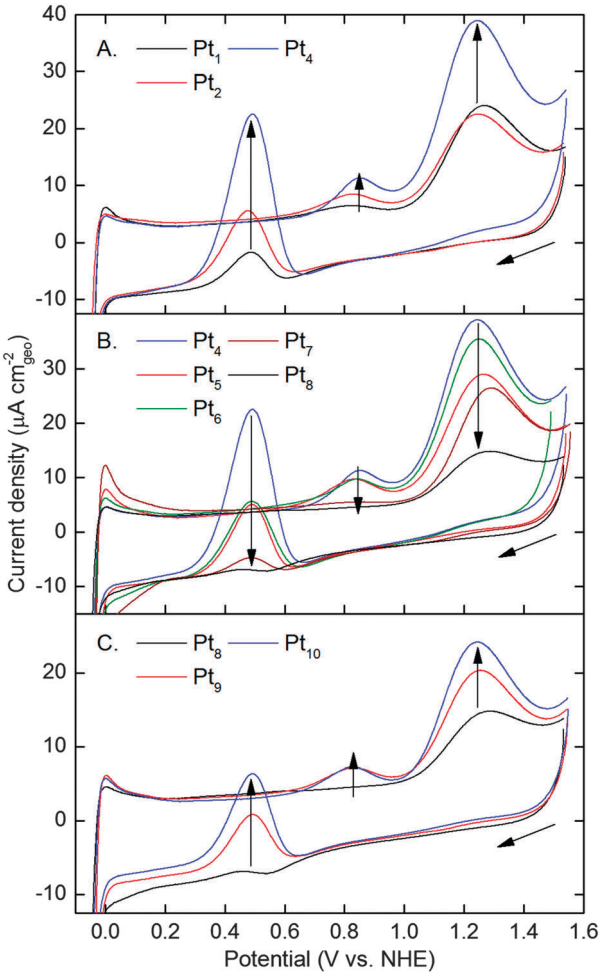

Fig. 5 CVs for Pt_n/ITO (n = 1, 2, 4–10), acquired at 0.1 V s^{-1} scan rate.

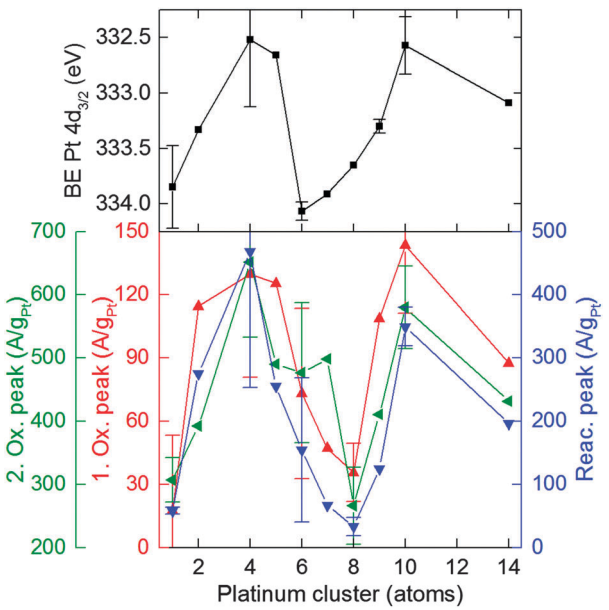

Fig. 6 Cluster size dependence of the Pt $4d_{3/2}$ BE (top, note inverted scale) and the background-subtracted peak EOR currents per gram Pt (bottom). Red: 1st oxidation peak, green: 2nd oxidation peak, blue: reactivation peak.

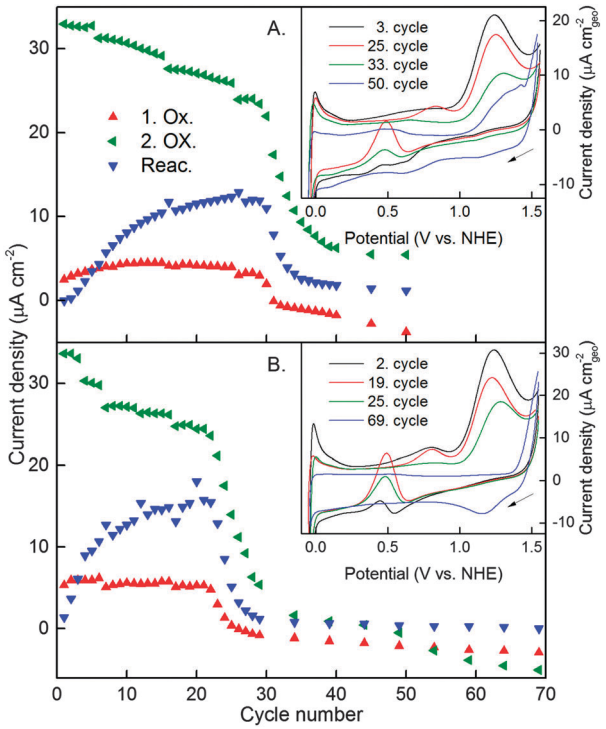

Fig. 7 Dependence of background-subtracted EOR current densities as a function of CV cycle number; (A) Pt_4/ITO. (B) Pt_{10}/ITO. Insets: raw CVs at selected points in the sequences, acquired at 0.1 V s^{-1} scan rate.

intensities slowed for the next 10 to 30 CVs, and then the EOR currents rapidly went to zero. As shown in the ESI,† this final rapid decline of EOR signals results from poisoning of the Pt_n/ITO by Cl^- diffusing from the reference electrode (Fig. S6, ESI†). The more gradual changes during the first 20–40 CVs could result from several effects of potential cycling. The ESI† shows that consumption of ethanol is negligible, however, we do expect the concentrations of reaction intermediates and products to change, both in the electrolyte and on the Pt_n/ITO surface. In addition, it is possible that potential cycling may induce restructuring of the Pt clusters.

Note, however, that the cluster size dependence, *i.e.*, the pattern of clusters with particularly high or low activities, is constant over the first 20 to 40 CVs (up to the point where poisoning sets in), and as discussed below, this precludes significant broadening of the size distribution during potential cycling.

Effects of air exposure on EOR activity

A Pt_4/ITO sample was prepared and studied as above, except that the antechamber was vented with air prior to starting electrochemical measurements. A sequence of 60 CVs was used to look at activity. All showed activity for HER and H_2 oxidation near 0.0 V and for OER at potentials above 1.4 V, as well as capacitive current from the ITO support. There was, however, no sign of EOR activity. Because ITO does not catalyze HER, OER, or H_2 oxidation in this potential range (Fig. 3), it is clear that the catalytic Pt sites were accessible for water electrolysis and H_2 oxidation, but EOR was apparently blocked by adventitious adsorbates. We were unable to restore EOR activity by potential cycling, but that may simply mean that Cl^- poisoning set in before the adventitious contaminants were removed.

Discussion

There are several interesting aspects of the results. From the perspective of size-selected electrochemical experiments, one important point is that activity varies non-monotonically by an order of magnitude with deposited cluster size, and the most active sizes (4 and 10) differ by only a few atoms from the least active (1 and 8) (Fig. 6 and Fig. S5, ESI†). Since all Pt_n/ITO samples had identical Pt coverages (4.40×10^{12} Pt atoms in the 2 mm spot), and the only parameter varied was the size of the deposited Pt_n, such strongly non-monotonic variation in activity with deposited size can only occur if the clusters remain mostly intact upon deposition and initial potential cycling. If sintering, dissolution or other processes that would broaden the size distribution were facile, the sharply oscillatory behavior would be averaged out, leaving at most a weak, monotonic variation in activity with size. The factor-of-ten variation in activity when size changes by only two atoms, suggests that the Pt_n must remain within an atom or two of the deposited size.

The size stability is striking, because the clusters were cycled through the Pt redox potential, and one might expect that this could lead to dissolution or electrochemically-driven diffusion and ripening, as has been seen for Pt clusters on carbon supports.[32] It is likely that the stability observed here reflects stronger interaction of the Pt_n with the ITO support, compared to the Pt–carbon interaction. Further evidence on this point comes from the Pt XPS BEs (Fig. 6), which show shifts relative to the value measured for bulk Pt (331.8 eV), ranging from 0.75 to 2.2 eV, compared to shifts of only 0.1 to 0.7 eV for Pt_n deposited on glassy carbon under similar conditions.[15] The larger shifts suggest that binding to ITO perturbs the cluster electronic environment more strongly than binding to carbon.

Another obvious conclusion from the size dependence, is that the chemistry responsible for ethanol electro-oxidation is possible even on Pt clusters containing just a few atoms. Indeed, Fig. 3 suggests that even isolated Pt atoms may catalyze some of the reactions, albeit with low efficiency.

While our static electrochemical cell makes it difficult to extract quantitative kinetics, it is interesting to compare the EOR activities for Pt_n/ITO with those measured for Pt_{poly} and Pt_{nano}/ITO under the same conditions. The comparison is given in more detail in the ESI.† Briefly, for Pt_{nano}/ITO and Pt_{poly}, the three EOR features are observed, peaking at ~0.9 V, ~1.35 V, and ~0.6 V, respectively, for the 1st and 2nd oxidation, and reactivation peaks. For samples prepared by depositing Pt_n, the corresponding peaks appear at somewhat lower potentials: 0.82–0.84 V, 1.24–1.28 V, and ~0.45–0.49 V, respectively. The most active samples, Pt_4/ITO and Pt_{10}/ITO, have peak currents per gram of Pt that are between ~5 and 15 times larger than those for Pt_{nano}/ITO, depending on the EOR peak in question. Even the less active Pt_n/ITO have currents per gram Pt that are

generally at least comparable to those for Pt_{nano}/ITO. High activity/mass is clearly valuable given the cost of Pt, and presumably reflects the fact that small clusters expose a larger fraction of Pt in the surface layer, compared to 5–10 nm particles.

Perhaps the most interesting observation is that the strongly size-dependent activity of the Pt_n/ITO electrodes is anti-correlated with the size-dependent Pt 4d BEs, suggesting that the electronic environment of the clusters is a controlling factor for EOR catalysis. The question is what this anti-correlation tells us about the relationship between electronic structure and activity. The 4d core electrons are not directly involved in the chemistry, however their BEs are sensitive to the valence electrons, which are. As discussed in the ESI,† BE shifts are often thought of in terms of the effects of the initial or final states of the photoemission process. In this case, both initial and final state perspectives lead to the conclusion that Pt_n/ITO which have particularly low Pt 4d BEs have Pt in an electron rich environment, while high BEs imply electron-poor Pt_n. Thus, electron-rich Pt_n/ITO are highly active as EOR catalysts, and electron-poor Pt_n/ITO are not.

This conclusion may seem counterintuitive, given that oxidation involves net transfer of electrons from reactant molecules to the Pt_n/ITO. The EOR process, however, requires activation of CH and OH bonds in ethanol, and OH bonds in water (the oxidant), and bond activation often involves transfer of electron density into anti-bonding orbitals associated with the bonds in question.[12] Anti-correlations between metal BEs and oxidation catalytic activity have also been seen for CO oxidation over Pd_n/TiO_2[33] and Pt_n/alumina[22] under gas-surface reaction conditions, and for electro-oxidation of carbon by water, catalyzed by Pt_n/glassy carbon.[15] In each case, it is possible to identify bond activation steps that might be enhanced by electron transfer from electron-rich clusters.

One final question is whether the oscillations in electronic structure and activity are inherent properties of the Pt_n or if they are strongly modified by interaction with the ITO support. The ESI† reviews the literature on spectroscopy and chemical properties of gas-phase Pt_n in different charge states. There is no clear relation between the size dependent properties of gas-phase Pt_n and Pt_n/ITO, however, the gas-phase literature does show that the charge state (anion, cation, neutral) of the clusters has a strong effect on reactivity. This conclusion is consistent with our observation that the electronic environment of the Pt_n, as influenced by binding the ITO, is a controlling factor in EOR activity.

Conclusion

We have shown that electrodes prepared by deposition of mass-selected Pt_n^+ on ITO have activity for ethanol oxidation that is strongly and non-monotonically dependent on deposited cluster size. Activity is anti-correlated with the Pt 4d BEs measured for the as-deposited electrodes, indicating that being in an electron-rich environment is a controlling factor in promoting EOR activity.

The fundamental results presented here suggest that the rates of inner-sphere redox reactions, and particularly, that for ethanol oxidation, can be tuned by controlling the electronic structure of the catalytic centers. In this example, electronic tuning was done by varying cluster size, however, other approaches, such as alloying or varying the metal–support interaction, may provide alternative routes to the same end. The high mass activity observed for certain cluster sizes suggests that small clusters might be an attractive target for high efficiency electrodes, if the clusters can be stabilized against sintering, poisoning, and dissolution.

Acknowledgements

This work was supported by the U.S. Department of Energy, Condensed Phase and Interfacial Molecular Science program grant no. DEFG03-99ER15003. The authors would like to thank the U. of Utah Chemistry machine shop for useful suggestions and construction of the electrochemical setup. We also are grateful to Matthew Neurock for helpful discussions.

Notes and references

1 S. C. S. Lai and M. T. M. Koper, Electro-Oxidation of Ethanol and Acetaldehyde on Platinum Single-Crystal Electrodes, *Faraday Discuss.*, 2008, **140**, 399–416.
2 F. Colmati, G. Tremiliosi-Filho, E. R. Gonzalex, A. Berna, E. Herrero and J. M. Feliu, Surface Structure Effects on the Electrochemical Oxidation of Ethanol on Platinum Single Crystal Electrodes, *Faraday Discuss.*, 2008, **140**, 379–397.
3 F. Vigler, C. Coutanceau, F. Hahn, E. M. Belgsir and C. Lamy, On the Mechanism of Ethanol Electo-Oxidation on Pt and PtSn Catalysts: Electrochemical and *in situ* Ir Reflectance Spectroscopy Studies, *J. Electroanal. Chem.*, 2004, **563**, 81–89.
4 R. A. Rightmire, R. L. Rowland, D. L. Boos and D. L. Beal, Ethyl Alcohol Oxidation at Platinum Electrodes, *J. Electrochem. Soc.*, 1964, **111**, 242–247.
5 L.-W. H. Leung, S.-C. Chang and M. J. Weaver, Real-Time Ftir Spectroscopy as an Electrochemical Mechanistic Probe. Electrooxidation of Ethanol and Related Species on Well-Defined Pt(111) Surfaces, *J. Electroanal. Chem.*, 1989, **266**, 317–336.
6 H. Wang, Z. Jusys and R. J. Behm, Ethanol Electrooxidation on a Carbon Supported Pt Catalyst: Reaction Kinetics and Product Yields, *J. Phys. Chem. B*, 2004, **108**, 19413–19424.
7 M. J. Giz and G. A. Camara, The Ethanol Electrooxidation Reaction at Pt(111): The Effect of Ethanol Concentration, *J. Electroanal. Chem.*, 2009, **652**, 117–122.
8 I. G. Casella and E. Desimoni, Xps, Sem and Electrochemical Characterization of a Platinum-Based Glassy Carbon Modified Electrode: Electrocatalytic Oxidation of Ethanol in Acidic Medium, *Electroanalysis*, 1996, **8**, 447–453.
9 J. F. Gomes, K. Bergamaski, M. F. S. Pinto and P. B. Miranda, Reaction Intermediates of Ethanol Electro-Oxidation on Platinum Investigated by SFG Spectroscopy, *J. Catal.*, 2013, **302**, 67–82.

10 F. Vigier, C. Coutanceau, A. Perrard, E. M. Belgsir and C. Lamy, Development of Anode Catalysts for a Direct Ethanol Fuel Cell, *J. Appl. Electrochem.*, 2004, **34**, 439–446.
11 A. Kowal, M. Li, M. Shao, K. Sasaki, M. B. Vukmirovic, J. Zhang, N. S. Marinkovic, P. Liu, A. Frenkel and R. R. Adzic, Ternary Pt/Rh/SnO_2 Electrocatalysts for Oxidizing Ethanol to CO_2, *Nat. Mater.*, 2009, **8**, 325–330.
12 M. Neurock, First-Principles Modeling for the Electro-Oxidation of Small Molecules, in *Handbook of Fuel Cells – Fundamentals, Technology and Applications*, ed. W. Vielstich, H. Yokokawa and H. A. Gasteiger, Advances in Electocatalysis, Materials, Diagnostics and Durability, John Wiley & Sons, Ltd, London, 2009, vol. 5.
13 S. St. John, P. Boolchand and A. P. Angelopoulos, Improved Electrocatalytic Ethanol Oxidation Activity in Acidic and Alkaline Electrolytes Using Size-Controlled Pt–Sn Nanoparticles, *Langmuir*, 2013, **29**, 16150–16159.
14 H. Wang, Z. Jusys and R. J. Behm, Ethanol Electrooxidation on Carbon-Supported Pt, Ptru and Pt_3Sn Catalysts – a Quantitative Dems Study, *J. Power Sources*, 2006, **154**, 351–359.
15 S. Proch, M. Wirth, H. S. White and S. L. Anderson, Strong Effects of Cluster Size and Air Exposure on Oxygen Reduction and Carbon Oxidation Electrocatalysis by Size-Selected Pt_n ($n \leq 11$) on Glassy Carbon Electrodes, *J. Am. Chem. Soc.*, 2013, **135**, 3073–3086.
16 K. J. Boyd, A. Lapicki, M. Aizawa and S. L. Anderson, A Phase-Space-Compressing, Mass-Selecting Beamline for Hyperthermal, Focused Ion Beam Deposition, *Rev. Sci. Instrum.*, 1998, **69**, 4106–4115.
17 A. von Weber, E. T. Baxter, H. S. White and S. L. Anderson, Cluster Size Controls Branching between Water and Hydrogen Peroxide Production in Electrochemical Oxygen Reduction at Pt_n/ITO, *J. Phys. Chem. C*, 2015, **119**, 11160–11170.
18 J. M. Thomas, Student Construction of a Gel-Filled Ag/AgCl Reference Electrode for Use in a Potentiometric Titration, *J. Chem. Educ.*, 1999, **76**, 97–98.
19 B. Rudy and L. E. Iverson, *Ion Channels – Reprint of Volume 207 in Methods in Enzymology Series*, Acad. Pr., New York, 1997.
20 H. Qiu, J. Yan, X. Sun, J. Liu, W. Cao, X. Yang and E. Wang, Microchip Capillary Electrophoresis with an Integrated Indium Tin Oxide Electrode-Based Electrochemiluminescence Detector, *Anal. Chem.*, 2003, **75**, 5435–5440.
21 J. Klett, S. Krähling, B. Elger, R. Schäfer, B. Kaiser and W. Jaegermann, The Electronic Interaction of Pt-Clusters with ITO and HOPG Surfaces Upon Water Adsorption, *Z. Phys. Chem.*, 2014, **228**, 503–520.
22 F. S. Roberts, M. D. Kane, E. T. Baxter and S. L. Anderson, Oxygen Activation and CO Oxidation over Size-Selected Pt_n/Alumina/Re(0001) Model Catalysts: Correlations with Valence Electronic Structure, Physical Structure, and Binding Sites, *Phys. Chem. Chem. Phys.*, 2014, **16**, 26443–26457.
23 A. N. Frumkin and E. A. Aikazyan, Kinetics of Ionization of Molecular Hydrogen on Platinum Electrodes, *Bull. Acad. Sci. USSR, Div. Chem. Sci.*, 1959, **8**, 188–197.
24 D. V. Savinova, E. B. Molodkina, A. I. Danilov and Y. M. Polukarov, Surface and Subsurface Oxygen on Platinum in a Perchloric Acid Solution, *Russ. J. Electrochem.*, 2004, **40**, 683–687.
25 A. J. Bard and L. R. Faulkner, *Electrochemical Methods: Fundamentals and Applications*, John Wiley and Sons, Hoboken, NJ, 2nd edn, 2001.
26 L. Benz, X. Tong, P. Kemper, Y. Lilach, A. Kolmakov, H. Metiu, M. T. Bowers and S. K. Buratto, Landing of Size-Selected Ag_n^+ Clusters on Single Crystal TiO_2(110)-1 × 1 Surfaces at Room Temperature, *J. Chem. Phys.*, 2005, **122**, 081102.
27 X. Tong, L. Benz, P. Kemper, H. Metiu, M. T. Bowers and S. K. Buratto, Intact Size-Selected Au_n Clusters on a TiO_2(110)-(1 × 1) Surface at Room Temperature, *J. Am. Chem. Soc.*, 2005, **127**, 13516–13518.
28 S. Lee, C. Fan, T. Wu and S. L. Anderson, Agglomeration, Sputtering, and Carbon Monoxide Adsorption Behavior for Au/Al_2O_3 Prepared by Aun + Deposition on Al_2O_3/NiAl(110), *J. Phys. Chem. B*, 2005, **109**, 11340–11347.
29 S. Lee, C. Fan, T. Wu and S. L. Anderson, Agglomeration, Support Effects, and CO Adsorption on Au/TiO_2(110) Prepared by Ion Beam Deposition, *Surf. Sci.*, 2005, **578**, 5–19.
30 S. Lee, C. Fan, T. Wu and S. L. Anderson, Cluster Size Effects on CO Oxidation Activity, Adsorbate Affinity, and Temporal Behavior of Model Aun/TiO_2 Catalysts, *J. Chem. Phys.*, 2005, **123**, 124710.
31 W. E. Kaden, W. A. Kunkel and S. L. Anderson, Cluster Size Effects on Sintering, CO Adsorption, and Implantation in Ir/SiO_2, *J. Chem. Phys.*, 2009, **131**, 114701.
32 K. Hartl, M. Nesselberger, K. J. J. Mayrhofer, S. Kunz, F. F. Schweinberger, G. H. Kwon, M. Hanzlik, U. Heiz and M. Arenz, Electrochemically Induced Nanocluster Migration, *Electrochim. Acta*, 2010, **56**, 810–816.
33 W. E. Kaden, T. Wu, W. A. Kunkel and S. L. Anderson, Electronic Structure Controls Reactivity of Size-Selected Pd Clusters Adsorbed on TiO_2 Surfaces, *Science*, 2009, **326**, 826–829.

